



## SOFT ROBOTS

# Stretchable Arduinos embedded in soft robots

Stephanie J. Woodman, Dylan S. Shah, Melanie Landesberg, Anjali Agrawala, Rebecca Kramer-Bottiglio\*

To achieve real-world functionality, robots must have the ability to carry out decision-making computations. However, soft robots stretch and therefore need a solution other than rigid computers. Examples of embedding computing capacity into soft robots currently include appending rigid printed circuit boards to the robot, integrating soft logic gates, and exploiting material responses for material-embedded computation. Although promising, these approaches introduce limitations such as rigidity, tethers, or low logic gate density. The field of stretchable electronics has sought to solve these challenges, but a complete pipeline for direct integration of single-board computers, microcontrollers, and other complex circuitry into soft robots has remained elusive. We present a generalized method to translate any complex two-layer circuit into a soft, stretchable form. This enabled the creation of stretchable single-board microcontrollers (including Arduinos) and other commercial circuits (including SparkFun circuits), without design simplifications. As demonstrations of the method's utility, we embedded highly stretchable (>300% strain) Arduino Pro Minis into the bodies of multiple soft robots. This makes use of otherwise inert structural material, fulfilling the promise of the stretchable electronic field to integrate state-of-the-art computational power into robust, stretchable systems during active use.

## INTRODUCTION

Arduinos and other single-board microcontrollers are reprogrammable, widely used, and have an open-source community comprising more than 1 million users (1), making their prevalence as controllers unparalleled in and out of the robotics world. Most soft robots today are controlled by Arduino-style microcontrollers (2–6). The modulus mismatch between rigid Arduino boards and the materials used in soft robots (for example, silicone elastomers) leads many designers to either place the electronics in regions of the robot designed to experience minimal strain (3) or off-board them entirely (7–9). Proposed solutions to this problem include mechanical computing platforms, soft logic gates, and stretchable electronics.

Instead of relying on conventional electronics, researchers have proposed fully soft mechanical computing platforms that exploit high-dimensional dynamic phenomena to perform computation and act as distributed information processing networks (10). Most of these non-von Neumann computational architectures take the form of tunable mechanical metamaterials that switch between two discrete states, analogous to binary digits (bits) in electronic computers. Soft logic gates have been proposed on the basis of fluidic principles [pneumatic (11, 12) and liquid (13, 14)], pointing toward fully autonomous open-loop behaviors such as locomotion and arm motion. However, these mechanical approaches lack the logic gate density to match the capabilities of traditional electronic computers, which have proliferated because of miniaturization and scaling.

Another approach toward embedded computation in soft robots is the field of stretchable electronics, where researchers aim to endow traditional computing platforms with stretchability. This approach retains the computational power density of traditional circuitry while introducing stretchable conductive traces and substrates that link silicon-based rigid integrated circuits (ICs). Stretchable traces made from geometric patterning of solid thin-film conductors (for example, serpentine or meshes) are known for excellent interfacing with

rigid microelectronics (15–18) but typically cannot reach the strains required for soft robot applications (20 to 1000% strain) (19). In contrast, stretchable traces made from liquid metals (LMs) (20, 21), LM composites (22–24), or conductive elastomers (25, 26) can often reach higher strains but, first, have difficulty interfacing with rigid IC components and, second, display strain-dependent electrical resistances.

Regarding the former, recent attempts have used acidic or alkaline solutions to improve the electrical conductivity of the IC-LM interface (27, 28). Tang *et al.* (29) presented an LM-adhesive mixture to promote substrate adhesion and IC interfacing, yet the inclusion of adhesive greatly reduced the formulation's conductance. Other works highlight how the interfaces between LM-based conductive inks and commercial ICs often suffer when strained, thus confining examples to low-strain demonstrations (27, 29–36) or simplified designs (27, 28, 33, 37). For example, Valentine *et al.* (38) proposed a non-commercial form, single-layer, microcontroller circuit but characterized only a simpler light-emitting diode (LED) circuit with LM interconnects under strain.

Regarding the latter, biphasic (solid-liquid) gallium-based formulations have been proposed as strain-insensitive conductors. Most biphasic metal formulations are made from a mixture of liquid eutectic gallium-indium (EGaIn) and solid metal particles [such as silver (31, 39, 40), copper (41), and nickel (42)] and yield favorable rheological properties for patterning, interfacing, and enhanced electrical performance. Formulations with added or natively formed semiconductive particles such as quartz (43), graphene oxide (44), and gallium oxide (37, 45) boast a suppressed strain response, an especially promising attribute for stretchable circuitry. We previously used biphasic gallium-indium (BGaIn), made from EGaIn with in situ formed crystalline gallium oxide ( $\text{Ga}_2\text{O}_3$ ) growth (~34 wt % of solid), to achieve high conductivity ( $2.06 \times 10^6$  S/m), extreme stretchability (up to 1000%), suppressed resistance changes when strained, cyclic stability (consistent performance over 1500 cycles), and a reliable interface with rigid electronics (37). However, this previous biphasic metal formulation was found to be laborious to produce at scale.

Department of Mechanical Engineering and Materials Science, Yale University, 9 Hillhouse Ave., New Haven, CT 06511, USA.

\*Corresponding author. Email: rebecca.kramer@yale.edu

In this work, we present material and interfacial processing solutions to previous challenges that enable a generalized end-to-end method for translating any two-layer circuit (such as an Arduino) into a soft stretchable form ready for integration into soft robots and wearable electronics (Fig. 1 and Movie 1). This method is made possible by, first, a scalable stretchable conductor with a suppressed strain response, cyclic stability, and reliable interfacing to ICs and, second, derived guidelines for conductor-substrate compatibility, which determines the reliability of the process. To demonstrate the utility of this method, we translated several open-source circuit designs containing ICs with dozens of interfaces and vertical interconnect accesses (VIAs) into stretchable forms and characterized their

function during high-strain cycling. We created a soft, stretchable Arduino Pro Mini that could be stretched to  $>300\%$  strain and maintain functionality for more than 120 cycles to 100% strain, despite having more than 70 interfaces between rigid and soft components and more than 40 VIAs. We further demonstrated the generality of the method by fabricating stretchable versions of the Arduino Lilypad, SparkFun Sound Detector, and SparkFun RGB (Red Green Blue) and Gesture Sensor. Notably, the circuits used the same form factor and IC packages as the originals, including both no-lead (for example, dual flat no-lead) and lead (for example, thin quad flat pack) packages. Last, we embedded stretchable Arduino Pro Minis into the bodies of soft robots at specifically high-strain locations and used

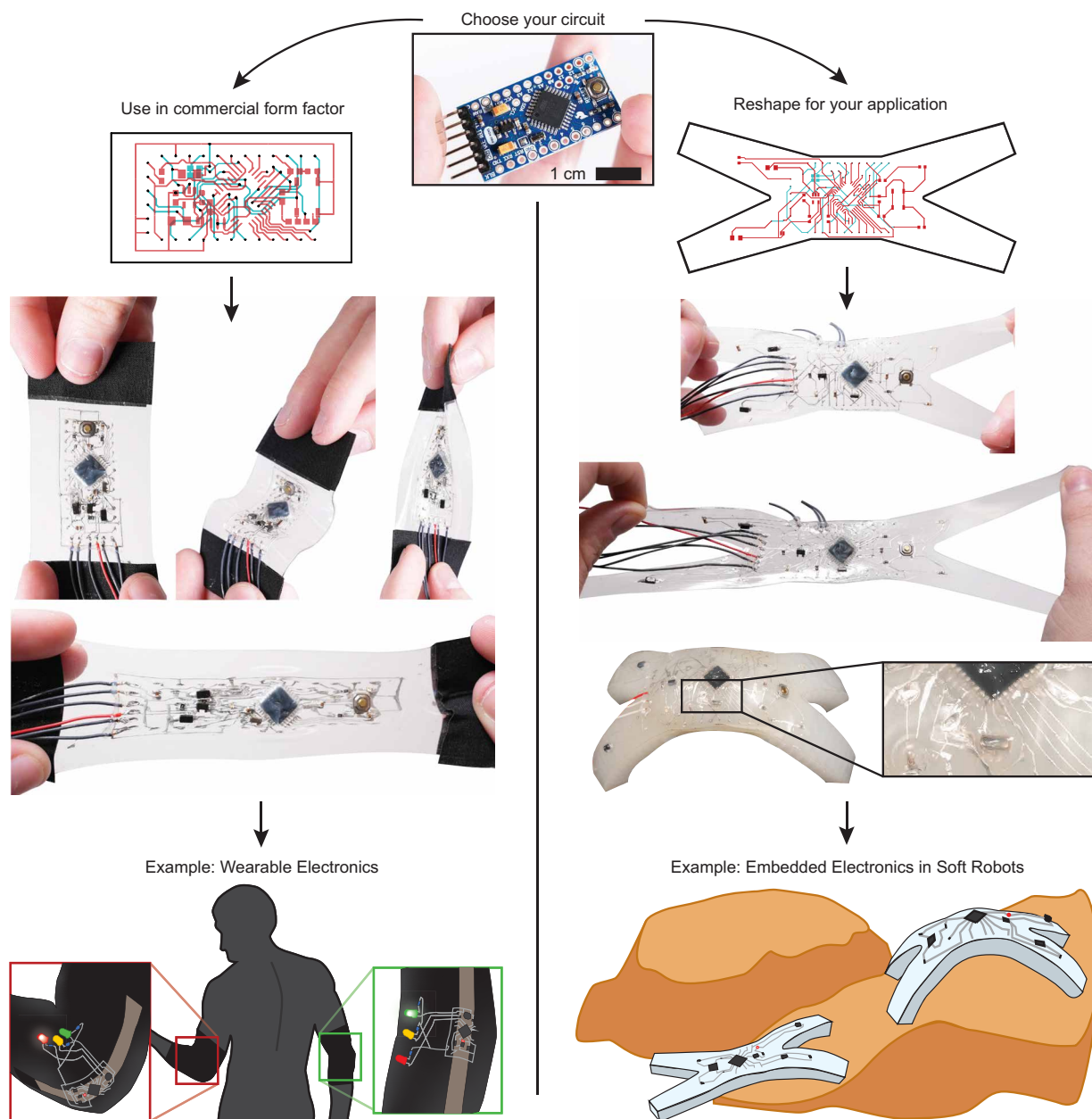
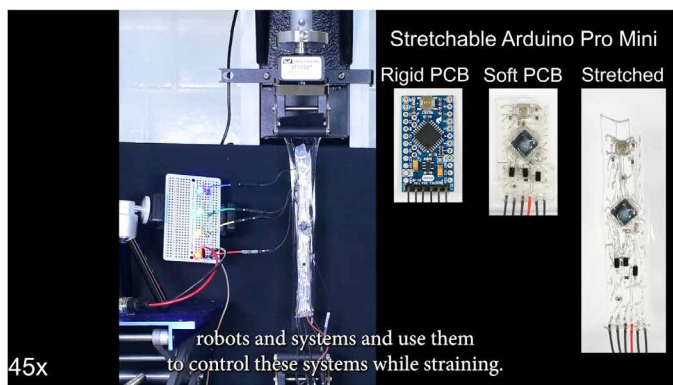


**Fig. 1. End-to-end method for translating complex commercial circuit boards into stretchable forms.** The method is enabled by biphasic conductors and tacked silicnes, enabling circuit integration into fully functioning wearables and soft robots during use.



**Movie 1. Stretchable Arduinos overview.** Using a biphasic (solid-liquid) EGaIn-based conductor, we created stretchable versions of several popular open-sourced circuits, including the Arduino Pro Mini. In this video, we show testing of the circuits and then embedding them into soft robotic systems to aid in sensing and control.

them for embedded computation. The demonstrations collectively mark a transition from one-off, functionally limited showcases to robust, reliable, and complex multilayer stretchable circuits.

## RESULTS

### Scalable, stretchable conductor with suppressed strain response

Recently, there has been much interest in so-called strain-insensitive stretchable conductors, which have a suppressed strain response relative to bulk conductor assumptions. In contrast, most traditional circuits use annealed copper traces (resistivity,  $1.72 \times 10^{-8}$  ohm-m; density,  $8.93 \text{ g/cm}^3$ ; at  $20^\circ\text{C}$ ). As a classical constant-conductivity bulk conductor, copper theoretically follows Pouillet's law (46) when strained

$$R/R_0 = (1 + \epsilon)^{1+2\nu} \quad (1)$$

where  $R/R_0$  is the relative (normalized) resistance change,  $\epsilon$  is the applied strain, and  $\nu$  is Poisson's ratio, which is most often assumed to be 0.5, implying that the conductor is incompressible (37). Although Pouillet's law predicts large increases in resistance even at moderate strains for bulk conductors, by engineering materials with stable conductance under large strains, stretchable complex circuits and low-loss power transmission can be achieved. Our previous work presented one such conductor with an electromechanical response suppressed far below that predicted by Pouillet's law—a BGaIn composition formed from semiconductive crystalline gallium oxide particles mixed with EGaIn (37, 45). However, BGaIn is labor intensive to produce, and the synthesis process yields small quantities per batch.

Another proposed biphasic conductor is oxidized gallium-indium (OGaIn) (47, 48), a biphasic foam containing amorphous gallium oxide particles and EGaIn. OGaIn is made via rigorous mixing of EGaIn in air and can be created at scale. In this study, we sought to rigorously characterize OGaIn in an attempt to replicate the desirable properties of BGaIn with a material that can be manufactured at a scale useful to industry. Despite the OGaIn and BGaIn materials having similar qualitative rheological characteristics, we measured OGaIn to be only 1.4 wt % of amorphous gallium oxide [close to the

1.21 wt % reported by Chen *et al.* (49)], whereas BGaIn was  $\sim 34$  wt % of solid crystalline gallium oxide (37). We surmised that OGaIn is primarily thickened through air inclusions (48), which are not accounted for in the weight percent of formulations. The density of OGaIn ( $4.65 \text{ g/cm}^3$  at  $20^\circ\text{C}$ ) was substantially lower than EGaIn's ( $>6 \text{ g/cm}^3$ ). Scanning electron microscope (SEM) micrographs, energy-dispersive x-ray spectroscopy (EDS), and x-ray diffraction analysis (fig. S1 and Supplementary Methods) suggested that the hardness of the gallium oxide that forms at the OGaIn-air interface prevents deformation of the air inclusions upon stretching, which could explain the observed viscosity enhancement of OGaIn relative to neat EGaIn. We further investigated the rheological properties of OGaIn, revealing its shear-thinning behavior, which suggests compatibility with extrusion printing techniques (fig. S2). Last, OGaIn and BGaIn exhibited similar bulk electrical conductivities of  $2.11 \times 10^6$  and  $2.06 \times 10^6 \text{ S/m}$  (37), respectively.

To assess the electromechanical performance, we patterned 250- $\mu\text{m}$  traces of OGaIn (as wide as the thinnest trace in the commercially available Arduino Pro Mini; see Materials and Methods and fig. S3A) onto an ASTM (American Society for Testing and Materials) D412 (50) standard dog-bone shape of acrylic foam tape [VHB (very high bond) tape, 3 M] that adheres strongly to IC packaging (fig. S3, B and C) and encapsulated the traces with rubber cement (Elmers Inc.). We then strained each sample to 400% strain (limited by our test setup). We found that the electromechanical response of OGaIn was below that predicted by bulk-conductor assumptions (Pouillet's law; Fig. 2A) (37, 46, 51). As one point of comparison, OGaIn had an  $R/R_0$  of 7 at 400% strain compared with 25 for a bulk conductor. Further, the  $R/R_0$  versus  $\epsilon$  behavior of OGaIn matched previously reported values for BGaIn in the range where comparison was possible (up to 100% strain) (45). To provide a more direct comparison, we additionally tested OGaIn and BGaIn on the same substrate and with the same trace width (fig. S4), finding similar agreement. OGaIn is thus a scalable replacement for BGaIn. To evaluate cyclic stability, we subjected single-trace samples [unstrained resistance of  $\sim 0.5$  ohm, which is consistent with previous literature (52, 53)] to 1000 cycles of 150% strain at 15 mm/min (Fig. 2B).

After an initial break-in period of a few cycles (54), the trace resistance increased by only  $\sim 0.5$  ohm between cycles 5 and 1000. To evaluate the interfacing stability between traces and rigid IC contact pads, we repeated the cyclic strain (Fig. 2C and fig. S3E) and high strain (fig. S5) tests with two traces bridged by a 0-ohm resistor (Digi-Key Inc.). There were no discernible differences between the interfaced and noninterfaced traces whether comparing the initial raw resistance or the resistance after cycling. This, along with contact resistance measurements (fig. S6), indicates that the slight increases in resistance observed with cycles are not attributable to interfacing. Possible sources of increased resistance may include an elongation of the trace length after stretching (because of viscoelastic properties and plastic deformation of the surrounding polymers) or a change in OGaIn's effective electrical conductivity (for example, through phase separation).

### Deriving guidelines for conductor-substrate compatibility

The wetting and adhesion of LMs and biphasic metals to a host substrate are important parameters in stretchable electronic applications (55, 56). In this work, we relied on the adhesion of OGaIn to both its underlying substrate and its colocated ICs. Given the cyclic stability shown in Fig. 2 (B and C), we inferred that this adhesion is

sufficient with the VHB tape. However, toward our goal of embedding complex stretchable circuits into the bodies of soft robots, we sought to characterize the adhesion of OGaln to other materials commonly used in soft robotics, in addition to probing how to modify existing materials to improve adhesion. Further, we selected substrate materials to derive a generalized correlation between OGaln-substrate adhesion and substrate material tack.

We compared a baseline VHB tape substrate with four silicone elastomer (Dragon Skin 10, abbreviated as DS10, SmoothOn Inc.) substrates with increasing fractions of a tactile mutator (Slacker, SmoothOn Inc.). We refer to the neat silicone elastomer as DS10, the formulation with a mixing ratio of 1:1:1 (part A:Slacker:part B) as Slacker 1, and formulations with mixing ratios (1:1.5:1) and (1:2:1) as Slacker 1.5 and Slacker 2, respectively. Further details can be found in Materials and Methods.

Our tests show a positive linear correlation ( $R^2 = 0.96$ ) between substrate tack and OGaln-substrate adhesion (Fig. 2D). All substrates had at least some OGaln adhesion, even with  $<0.1$ -N tack, which is likely due to the oxide particle inclusions in OGaln (55) that encourage wetting (56). In practice, we found that substrates with low tack values (such as neat DS10 and Slacker 1 in Fig. 2D) increased the likelihood of failure modes (such as trace defects and IC shifting; table S1). Therefore, we recommend selecting substrates

with a tack value of at least 0.18 N to ensure sufficient OGaln-substrate adhesion, stable IC placement, and general conductor-substrate compatibility for stretchable circuits.

### Translating complex circuits into stretchable forms

Having identified a suitable stretchable conductor and generalized its compatibility with soft, stretchable substrates, we then developed a method of translating the as-is, complex circuit-board designs into stretchable circuits. Throughout the development of the method reported herein, we emphasized accessibility, aiming to eliminate a need for extensive equipment or materials expertise or circuit design expertise. We applied the method to make stretchable versions of the popular Arduino Pro Mini, a reprogrammable single-board microcontroller, as well as the Arduino Lilypad, SparkFun Sound Detector, and SparkFun RGB and Gesture Sensor.

The circuits were fabricated using laser cutting and stencil printing (Fig. 3). The substrate (for example, VHB tape) was sandwiched between two layers of 0.1-mm-thick sticker paper that acted as a mask. The main trade-off we noted in selecting the sticker paper was that thinner paper allowed for more precise traces, whereas thicker paper facilitated easier removal and reduced smearing of traces because of ripping. The board outline and VIAs were cut using a carbon dioxide (CO<sub>2</sub>) laser (Universal Laser VSL 2.30DT), and the trace outlines were etched on the bottom mask

using an ultraviolet (UV) laser (LPKF Protolaser U4). OGaln was painted onto the bottom traces, the mask was removed, and the circuit was encapsulated with a thin layer of rubber cement (Elmers Inc.). Next, the top traces were made using the same laser and painting procedure, followed by component placement and a rubber cement sealing step. Last, silicone adhesive (Sil-Poxy, SmoothOn Inc.) was added to a small region around the microprocessor to reduce stress caused by the stiffness gradient. For full process details, we refer the reader to Materials and Methods. In contrast with our more restrictive prior art that used transfer printing (37), this scalable screen-printing- and laser cutting-based process enables the creation of encapsulated multilayer circuits using substrates that meet the compatibility requirement (tack  $\geq \sim 0.18$  N) and can accommodate dense IC components while withstanding high strains. Furthermore, increased adhesion led to increased robustness of the IC-OGaln interfaces, allowing us to directly transfer commercial circuits into stretchable forms.

Straining the soft Arduino Pro Minis to failure (defined as a disconnection of serial communication to the computer; see Materials and Methods, Fig. 4, A to C, and movie S1; strain rate, 15 mm/min), we found that serial disconnect always occurred because of loss of electrical contact or shorting of the traces before mechanical failure of the substrate. The average strain at serial disconnect was 328%, with

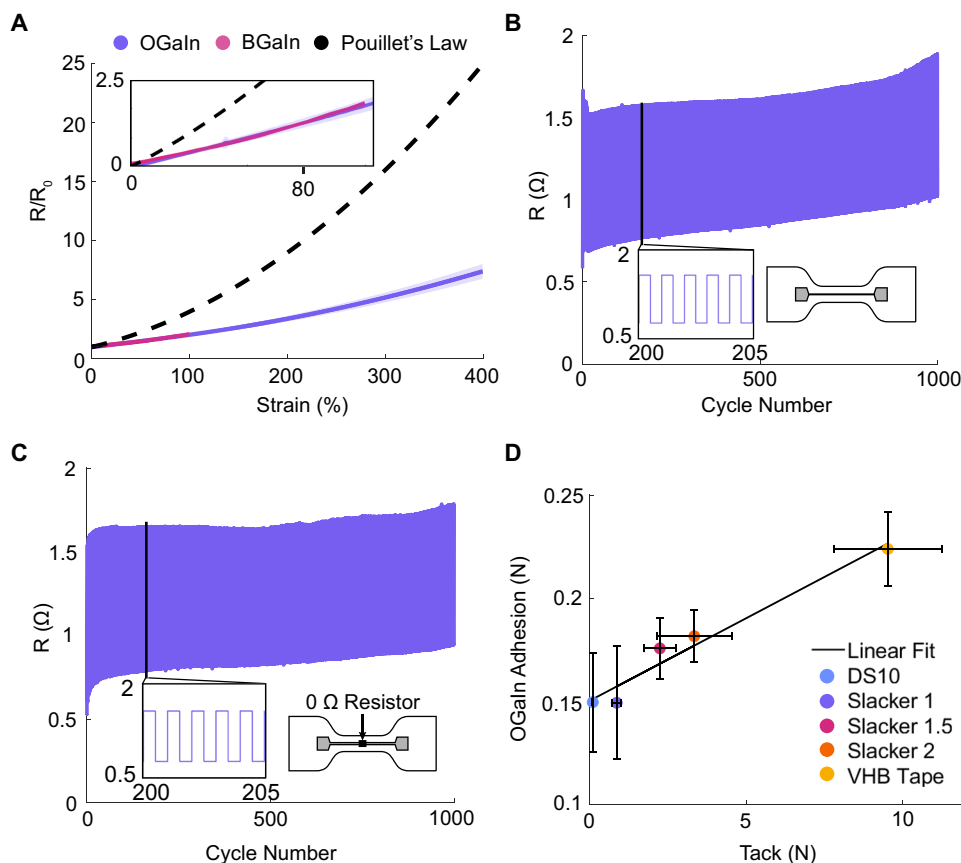


**Fig. 2. OGaln characterization and substrate compatibility.** (A) Normalized resistance change versus strain for five OGaln samples, plotted alongside the theoretical values for a bulk conductor and previous results from our BGaln alloy (45). Shaded regions represent one SD. (B) Representative electrical resistance versus cycle number for an OGaln trace stretched to 150% strain over 1000 cycles. (C) Representative electrical resistance versus cycle number for an OGaln trace with a 0-ohm resistor stretched to 150% strain over 1000 cycles. (D) OGaln adhesion versus ASTM D6195-22 tack measurement of various stretchable substrates. Error bars indicate one SD from the mean over five trials.

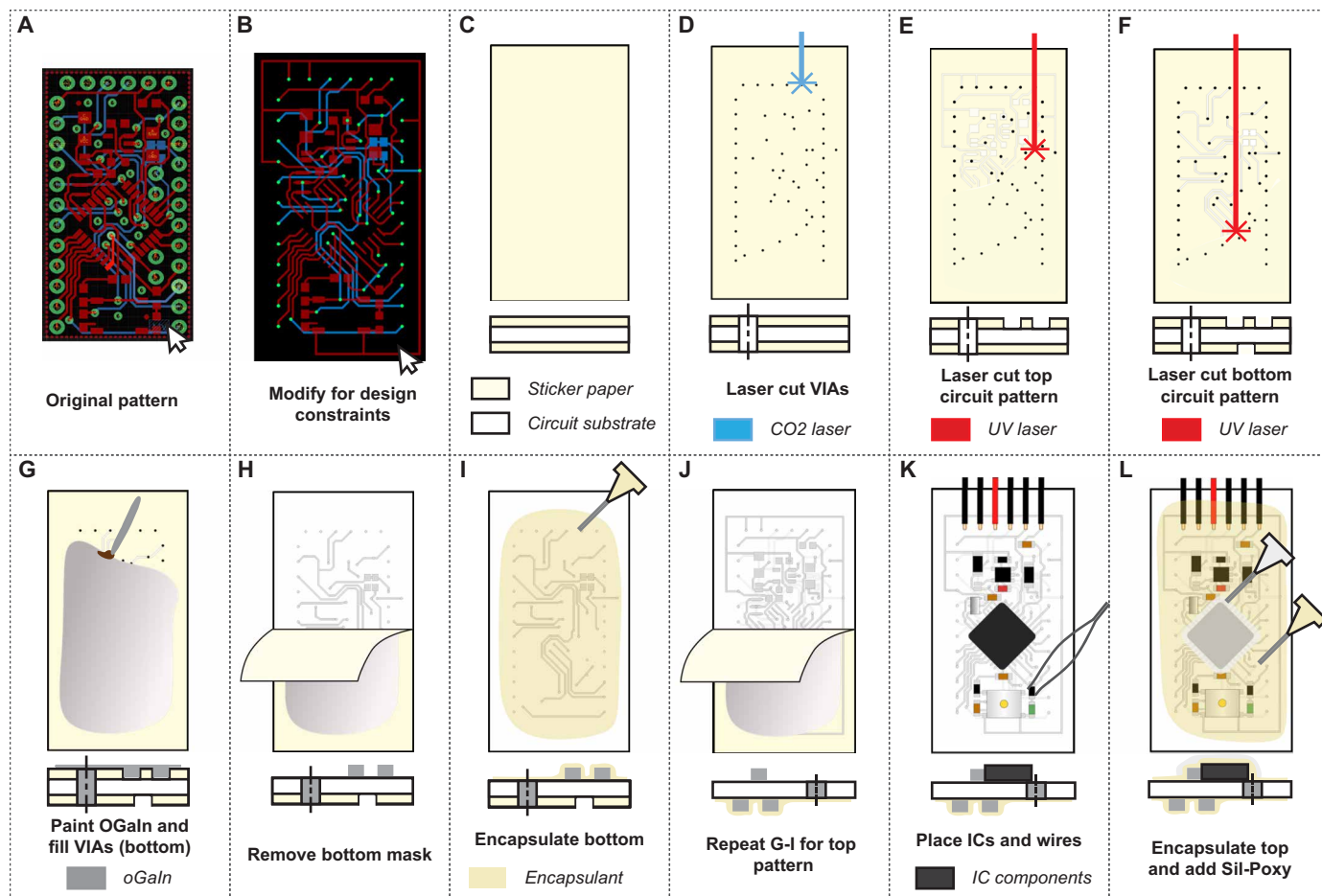


**Fig. 3. Circuit manufacturing.** (A) Original, open-source Arduino Pro Mini file in Autodesk Eagle. (B) Modified circuit design ready for laser cutting. (C) Circuit substrate sandwiched between sticker paper. (D) Laser cut board outline and VIAs in sticker paper with CO<sub>2</sub> laser. (E) Cut top layer of circuit traces using UV laser. (F) Cut bottom layer of circuit traces using UV laser. (G) Paint bottom traces and fill VIAs with oGaln. (H) Remove bottom mask and test trace conductivity. (I) Encapsulate with material of choice. (J) Paint top traces with oGaln and remove mask. Test trace conductivity. (K) Place components and wires. (L) Encapsulate top. Add Sil-Poxy around microprocessor.

the five samples failing between the range of 202% strain and 404% strain, corresponding to a failure in the plastic regime of each force-displacement curve (Fig. 4D). For two of the five samples tested, the circuit no longer functioned after returning to the unstrained state. However, two samples rebooted in an error state (no serial communication), and one sample remained reprogrammable after being strained past initial serial disconnect.

Cycling the Arduinos to 100% strain (rate of 15 mm/min) demonstrated stability over at least 100 cycles, with the average number of cycles at failure being 124 and one sample reaching 200 cycles before failure (Fig. 4E). For cyclic testing, circuits would be functional until an initial failure and not recover after that first failure even when unstrained. Force versus strain curves for neat substrates (VHB) and circuit-embedded substrates reveal that the circuits have a slight bulk stiffening effect on their host materials, although this appears to diminish with further cycling (Fig. 4F). After 200 cycles, the materials exhibited similar behavior, with the force at 100% strain only 27% higher for the circuit compared with neat VHB. Both cycles exhibited similar plastic deformation after the first cycle (the Mullins effect) (57).

Posttest analysis revealed that the strain-limiting Sil-Poxy region around the microprocessor, although it prevented shorting between microprocessor pins, introduced the most common failure mode of trace bridging at the edge of the strain-limiting region (fig. S7). This result suggests that the soft circuits could be improved by introducing stiffness gradients into the substrate (58). Another failure mode observed was at the trace-IC interface, indicating that enhancing the interfacial electrical connections could extend the operational strain range of the circuits. In addition, two trace failures were observed during cyclic testing, seemingly unrelated to a rigid-soft interface. These failures are suspected to be caused by trace thinning because of viscoelastic effects.

To ensure generality with respect to commercial circuit design and IC package types, we stretched to failure one sample each of the Arduino Lilypad, SparkFun Sound Detector, and SparkFun RGB and Gesture Sensor (Fig. 5 and movie S2). The Lilypad, whose rigid counterpart was specifically intended for wearable applications, strained to 415% before slipping out of its mount while still functioning (Fig. 5A). The Sound Detector, which is an analog circuit containing a through-hole mounted microphone, strained to a

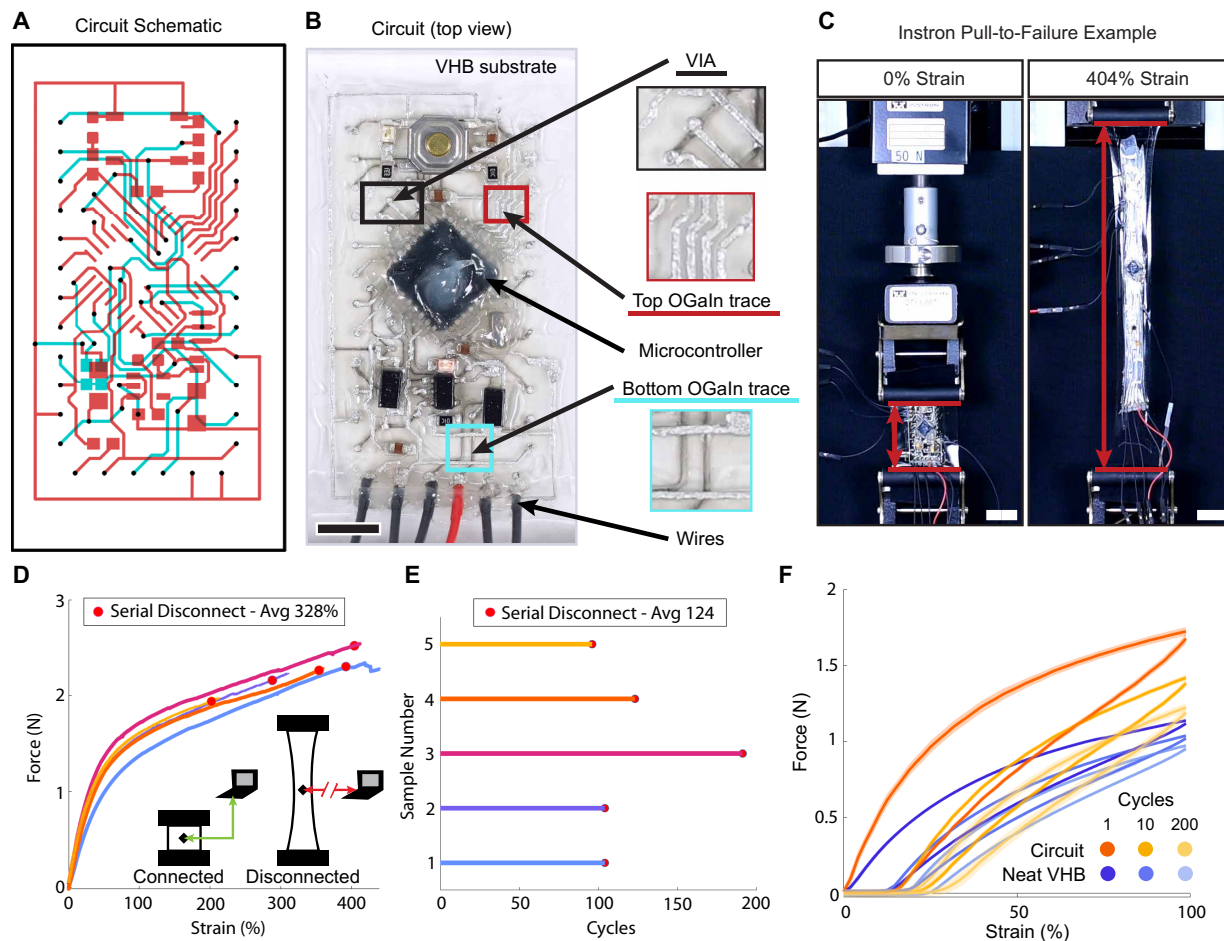


**Fig. 4. Circuit characterization.** All circuits in this figure used VHB tape as a substrate. **(A)** Circuit schematic showing top and bottom traces in red and cyan, respectively, and VIAs in black. **(B)** Identifying key circuit components and materials. Note that the top and bottom interconnect layers can be seen because VHB tape is translucent. In addition, the VIAs can be seen as round dots at various locations on the interconnects. Scale bar, 5 mm. Trace widths in insets are 0.25 mm. **(C)** Image of circuit before strain testing on the materials testing system (Instron 3345) and just before serial disconnect at 404% strain. Scale bars, 18.8 mm. **(D)** Force versus strain curves for each sample when strained until serial disconnect, noting when serial disconnect occurred for each sample. **(E)** Cycle number when serial disconnect occurred for each sample, when the circuit was repeatedly strained to 100%. **(F)** Comparing cyclic behavior of neat VHB tape (circuit substrate material) and the circuit at 1, 10, and 200 cycles. Solid lines are means over five samples after the number of strain cycles indicated in the legend. Shaded area indicates one SD.

lower strain of 258% (Fig. 5B). Last, the RGB and Gesture Sensor only uses no-lead IC packages, endowing it with higher stretchability, and it strained to 442% without failure (Fig. 5C).

### Soft robots with embedded soft computers

The soft Arduino Pro Minis were embedded into three soft robotic systems where, first, an Arduino controlled the gait of a locomotive robot; second, an Arduino sensed and communicated physical contact between agents in a multirobot system; and, third, an Arduino categorized the stretch data (low, medium, and high) and visually indicated the user's motion in a wearable system (Fig. 6).

#### Onboard pneumatic control of a quadruped soft robot

We first aimed to demonstrate how soft single-board microcontrollers, and by extension other complex circuits, can be embedded into the structural material or unused surface area of soft robots—even at high-strain locations. We fabricated stretchable Arduino circuits on, first, a silicone substrate (Slacker 1.5) (Fig. 6A), which matches the material of a silicone robot, and, second, a VHB tape substrate

(Fig. 6B) and integrated them into a canonical quadrupedal soft robot form factor (see Materials and Methods) (3, 8). In both cases, the microprocessor IC was integrated into the robot at the location of the highest strain during robot locomotion. The onboard soft Arduino was powered by a USB (universal serial bus) cable and used an I<sup>2</sup>C (interintegrated circuit) to command off-board pressure regulators (59) to inflate the actuators and generate a forward walking gait (Fig. 6C). The soft Arduino achieved successful processing and external communication at maximum strains of ~100% (movies S3 and S4). The soft Arduinos featured a custom layout in this demonstration, while keeping the most delicate components in the area of highest strain, to showcase that design modifications can be made to tailor-fit the host robot (Fig. 1).

#### Neighbor-neighbor sensing in a multiagent system

To illustrate scenarios where embedded computation could enable new capabilities in mobile soft robots, we integrated soft Arduinos into the surface of fully stretchable, pneumatic VoxelBots (60, 61). Notably, the VoxelBots contain no strain-limiting surfaces, precluding

rigid onboard printed circuit boards (PCBs) and requiring all included circuitry to be stretchable. This multiagent demonstration is a step toward our vision of a cell-like, modular approach to distributed computation, wherein robot modules may reconfigure relative to one another as a form of global shape change (62).

The VoxelBots were created by casting hollow cubes of silicone (DS10), bonding them together using silicone, inserting pneumatic tubing, and attaching stretchable VHB-based Arduinos using DS10 (see Materials and Methods). To implement a visual output, we additionally added a stretchable LED board (fig. S8) connected to the Arduino (Fig. 6D) embedded into the surface of the VoxelBot. Last, to allow each VoxelBot to sense contact with other VoxelBots, one of the

Arduino's analog pins was connected to an exposed OGaIn trace on one of two front faces on the robot. The other face, on the bottom, contained an exposed OGaIn trace connected to the Arduino's ground (GND) pin. The completed VoxelBots were then sequentially inflated and deflated using compressed air to locomote toward each other over approximately 30 steps (Fig. 6E), and the onboard soft Arduino was programmed to sense and report contact with the other VoxelBots. When the input pin (A3) and GND pins on each robot made contact, their embedded Arduinos detected the voltage change and lit the VoxelBots' green LED to indicate successful contact (Fig. 6F and movie S5).

#### Colocated computation and sensing in a wearable system

Given that the maximum strain of the stretchable Arduinos (on average, 300%) far exceeds the maximum strain experienced by the human body (~75% strain) (63), they can be placed nearly anywhere on smart garments. In contrast with previous works that use stretchable conductors as strain sensors and locate the IC interfaces in low- or no-strain locations (29, 36, 38, 64), we intentionally placed our soft Arduino on the high-strain elbow skin (Fig. 6G). We pressed a VHB-based Arduino and accompanying LED board (fig. S8) onto a Spandex elbow sleeve (using the VHB tape and rubber cement's natural adhesion) with an embedded textile capacitive strain sensor (Fig. 6G) (65). Red, yellow, and green LEDs were attached to three pins of the stretchable Arduino (see Materials and Methods).

The Arduino was programmed to convert voltages from the sensing board to capacitance and print capacitance values to the serial port. Simultaneously, the Arduino indicated the strain range by lighting up the green, yellow, or red LEDs (Fig. 6H and movie S6). The red LED indicated a high strain (>80 pF), yellow indicated a middle range (78 to 80 pF), and green indicated little or no strain (<78 pF). Capacitance increases with strain because of an increase in surface area of the parallel plate electrodes (65). Overall, this demonstration highlights the design freedom enabled by high-strain interfaces with respect to circuit placement.

#### DISCUSSION

We presented a generalized, scalable, accessible, end-to-end method to translate complex two-layer circuits into soft, stretchable forms. We used and characterized a biphasic stretchable conductor with a suppressed strain response, cyclic stability, and robust interfacing to ICs and determined that substrates with a tack of  $\geq 0.18$  N are necessary for conductor-substrate compatibility. These revelations together allowed us to introduce a commercial-form stretchable Arduino. We further made stretchable forms of other commercial circuits, from the popular vendors Arduino and SparkFun, that show the breadth and generality of the method to a wide range of open-source, commercially available designs.

We integrated stretchable Arduino Pro Minis into several soft robotic systems in locations where they experienced >100% strain. These integrations demonstrated soft locomotion quadrupeds with embedded electronics to control gait, a fully soft two-agent robotic system using onboard, stretchable control and sensing, and detection of a user's arm motion in a smart garment with the stretchable circuit intentionally placed in the area of the highest strain. The simplicity, accessibility, and success of the stretchable circuit fabrication method described herein give it the potential to be widely adopted by researchers, hobbyists, and those in industry. All of our circuits are based on open-source designs, and our design files used

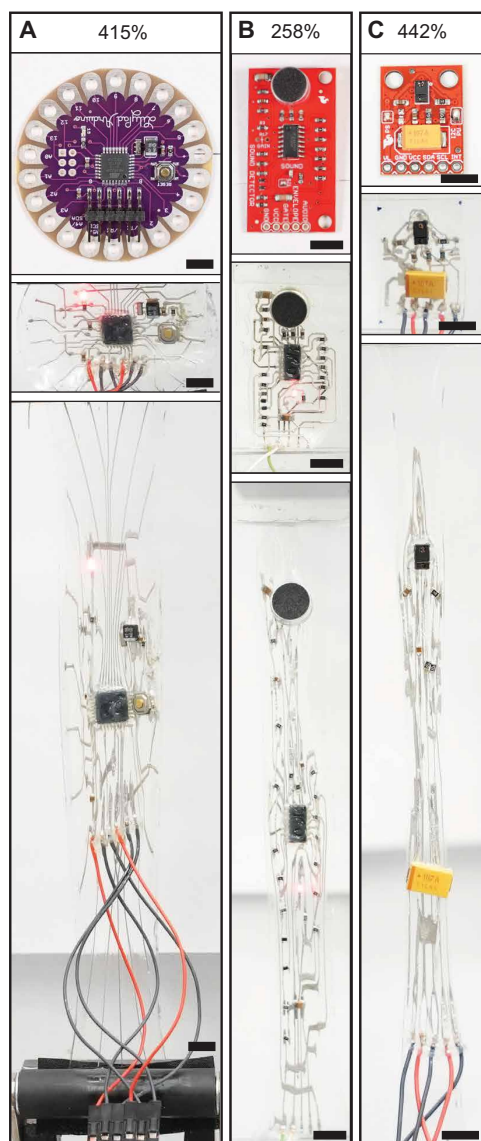


**Fig. 5. Additional circuits.** (A) Arduino Lilypad in rigid and soft form at 0% strain and the soft form at 415% strain. Scale bars, 7 mm. (B) SparkFun Sound Detector in rigid and soft form at 0% strain and the soft form at 258% strain. Scale bars, 9 mm. (C) SparkFun RGB and Gesture Sensor in rigid and soft form at 0% strain and the soft form at 442% strain. Scale bars, 9 mm.

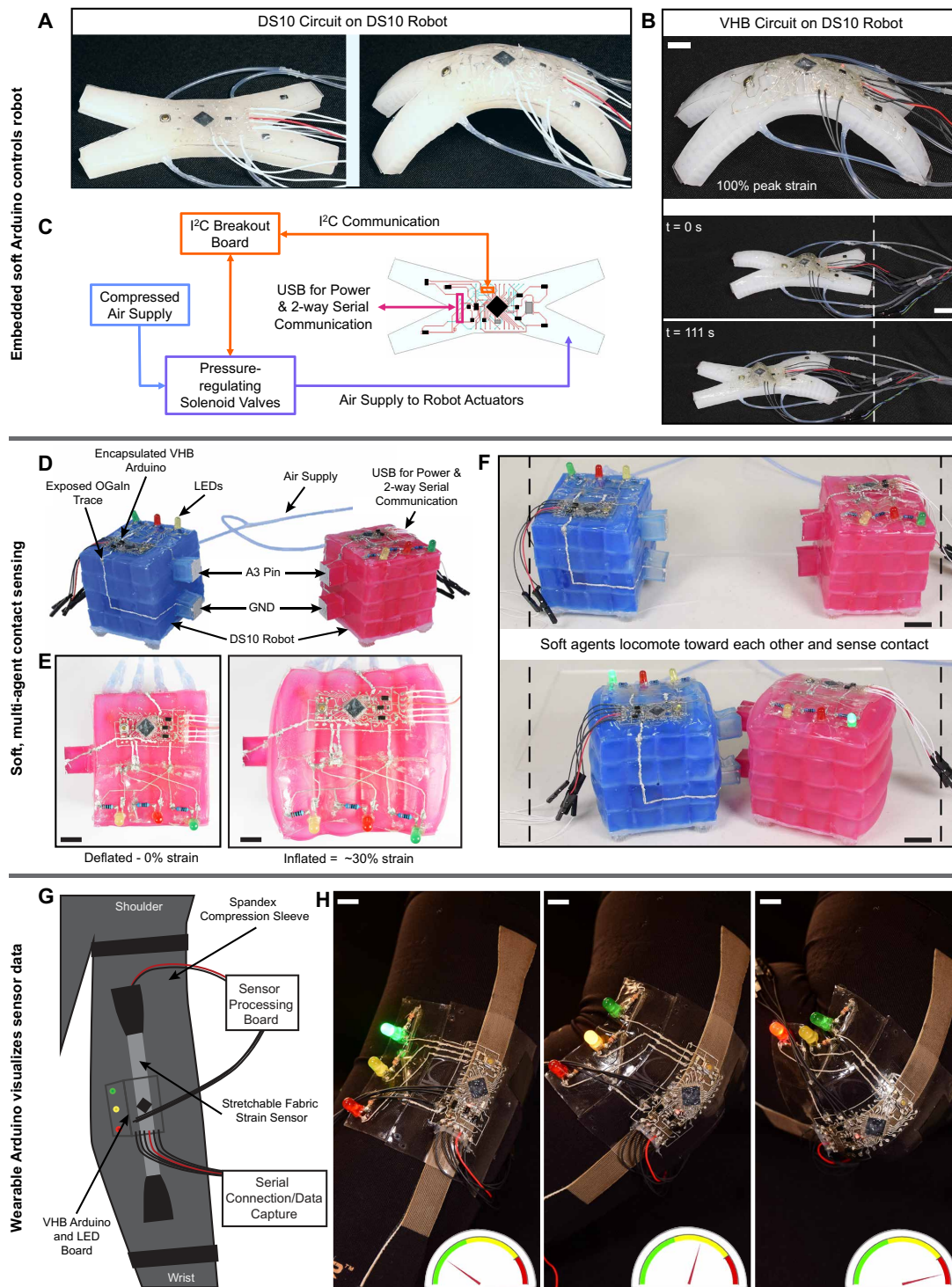


**Fig. 6. Embedded computation in soft systems.** (A) Silicone circuit embedded in a silicone (DS10) robot before it takes a step and mid-step, in a location where the circuit experiences  $\sim 100\%$  strain. (B) A circuit with VHB as the substrate is mated to a DS10 robot at full inflation and at different times during the walking gait. Scale bars, 8 mm. (C) Schematic of the quadruped driven by its embedded Arduino. (D) Stretchable Arduinos used for contact sensing in a two-robot system. (E) Top view of the robot before and after inflation (before taking a step and mid-step). Scale bars, 8 mm. (F) Robots' initial poses and after they make contact. Scale bars, 10 mm. (G) Stretchable Arduinos integrated with sensing circuitry in a smart garment that senses the user's elbow bending motions. (H) Sequential images showing a user bending their elbow and the Arduino detecting the motion as displayed by the gauge. Scale bars, 7 mm.

to create the masks have been made available in our accompanying GitHub repository.

Our long-term goal is to develop stretchable versions of a wide range of familiar circuits (for example, within the Adafruit and SparkFun communities), advancing the field of soft robotics and wearables and lowering the barrier to entry into soft robot research by enabling the use of common control platforms. Important functionalities could be added to make the robots more self-contained, such as Bluetooth modules and flexible/stretchable batteries to reduce external wiring requirements and soft valves to bring additional pneumatic capabilities onboard. The process could be further tested to determine Gerber-like style guidelines, which could then be added into common design software (such as Eagle or Altium) to determine design viability in stretchable form. In addition, we hope that this technique will be adopted by vendors of proprietary circuits, alongside an industry-academia joint effort to develop standardized connectors analogous to Qwiic (SparkFun Inc.) or USB connections from rigid electronics.

Future work will include further improving maximum circuit strains, possibly through increased substrate tack or surface treating the ICs with adhesion promoters. We also aim to reduce the manufacture time using commercial stencil-printing machines for the traces, nozzle dispensing for VIAs (42), and automated pick-and-place machines for the ICs. We hope that this work will enable further research into soft systems endowed with computational intelligence rivaling today's rigid systems without sacrificing compliance, thus facilitating the realization of soft robots that can sense, decide, act, and adapt in the real world.

## MATERIALS AND METHODS

### OGaIn fabrication and characterization

OGaIn was fabricated by measuring 200 ml of EGaIn into a 250-ml glass beaker and mixing using an IKA Eurostar 20 digital mixer, with a four-blade stainless steel propeller, for 30 min (fig. S3A). Resistivity and conductivity were estimated by measuring the resistance of a trace with known length, width, and height using a four-point probe multimeter (B&K Precision). The weight percent of solid particles was measured by weighing a sample of OGaIn before and after dissolving the solid particles in 12 M HCl.

The density was measured by weighing a known volume of OGaIn. A 2.54 cm-by-2.54 cm-by-0.64 cm mold was precision-cut from acrylic using a laser and then securely clamped to another acrylic piece. The weight of the empty mold was recorded. OGaIn was carefully applied into the mold using a wooden craft stick, ensuring thorough filling of corners and the absence of air gaps. Excess material was removed by drawing the craft stick across the mold's top. The filled mold was weighed again, and the OGaIn density was calculated by subtracting the empty mold weight from the filled mold weight and dividing by the known volume. We measured the density of three samples and reported the mean.

X-ray diffraction testing was completed on a Rigaku SmartLab machine with a 2-mm window. SEM images were taken on a Hitachi CFE SU8230. EDS analysis was performed with a Bruker QUANTAX FlatQUAD (mapping at 5 kV and compositional analysis at 6 kV). Surface samples were prepared on 12.5-mm stubs on carbon tape. Cross-sectional samples were prepared on vertical sample holders on carbon tape, where a trace of OGaIn was frozen and then broken in half and mounted to the stub. Stretched cross sections were

prepared by casting OGaIn on VHB, encapsulating with rubber cement, and then stretching the substrate while applying to the SEM stub. After mounting the sample, it was frozen and then broken to reveal the stretched cross section.

The single-trace samples were created using the dimensions and electrode attachment techniques described in (45), with VHB tape and rubber cement as the substrate and encapsulant, respectively. The trace widths of OGaIn were 250  $\mu\text{m}$ , with a gauge length of 25 mm (fig. S3, B and C). Resistor samples of 0 ohm were made using the same patterns and processes but with a 0.25-mm gap in the middle of the trace, over which a 0402 0-ohm surface-mount resistor was placed (fig. S3E). The single-trace samples were characterized using the custom setup previously described in (45) and illustrated in fig. S3D. An Arduino-driven lead-screw actuator controlled the strain and strain rate, and resistance was recorded using a four-point probe multimeter (B&K Precision).

### Substrate viability characterization

ASTM D6195-22 standard tack testing was carried out using an Instron 3345 tensile tester (maximum capture rate, 2 ms; fig. S9A). Five samples of each material were created as follows: VHB tape was adhered to the polyethylene terephthalate backing, ensuring that no air bubbles were present. The DS10 (Dragon Skin 10A, SmoothOn Inc.) samples were made by casting DS10 over the polyethylene terephthalate backing with a 0.5-mm draw bar. That same technique was used to create the samples of Slacker 1, Slacker 2, and Slacker 3. Slacker 1 used one part DS10 part B, one part Slacker (SmoothOn Inc.), and one part DS10 part A (denoted 100:100:100). Slacker 1.5 used the ratio 100:150:100, and Slacker 2 used 100:200:100.

The same setup, sample creation, and procedure were used for the OGaIn adhesion as for the previously described tack testing, although, instead of coming into contact with steel, the samples came into contact with molded OGaIn (fig. S9, B to E). A 25 mm-by-25 mm-by-1.59 mm-deep mold was created to fit onto the steel bar used for previous experiments (fig. S9B). This mold was filled with OGaIn before each new sample, and a bar was drawn across the top surface before removal of the mold (fig. S9C).

To get an application-based analysis of the effects of OGaIn-substrate adhesion on the circuit manufacturing process, defect rate tests were carried out. Five traces (250  $\mu\text{m}$  in width and 45 mm in length) of OGaIn were screen-printed onto each of the substrates (VHB tape; DS10; Slacker 1, Slacker 2, and Slacker 3) using a sticker paper mask. The conductivity of each trace was measured, and a binary rating of conductive or nonconductive was recorded for each trace (table S1).

### Stretchable Arduino Pro Mini manufacturing

The circuit pattern for the Arduino Pro Mini was downloaded from Arduino.com in the industry-standard Eagle PCB design file format. The relevant circuit layers—bottom, top, VIAs, and header pin holes—were exported to CorelDRAW for postprocessing and to prepare the files for laser cutting (Fig. 3A). In CorelDRAW, GND lines were added to replace the commercial PCB's GND pour. VIAs and header pin hole sizes were reduced to 0.4 mm in diameter (Fig. 3B). The reduction in VIA size from the open-source design to the soft design left sufficient clearance between the VIAs and traces, as well as the header pins and traces. The implemented circuits also featured a minimum trace width of 0.2 mm, a minimum clearance between VIAs and traces of 0.29 mm, and a minimum distance between traces of 0.17 mm.

Here, we detail the manufacturing procedure illustrated in Fig. 3 and recorded in movie S7. Although Fig. 3 presents a general procedure, this text will use VHB tape (VHB 4905, 3M Inc.) as the circuit substrate and rubber cement (Elmers Inc.) as the encapsulant. If a DS10/Slacker circuit was desired, we replaced the VHB tape with a cured 0.5-mm casting of Slacker 1, Slacker 1.5, or Slacker 2 and replaced rubber cement with uncured Slacker 1, Slacker 1.5, or Slacker 2. To compare each material's stiffness, we measured the 100% modulus of all materials used in this manufacturing process following ASTM D412-16, with dog-bone type C (fig. S10). Briefly, the modulus of Sil-Poxy  $E_{sp}$  was about four times that of DS10 ( $E_{DS10}$ ), which was similar to those of VHB and rubber cement, followed by Slacker 1, Slacker 1.5, and Slacker 2 being  $<0.2 \times E_{DS10}$ .

First, sticker paper from the back of double-sided tape (Le Papillon Jewelry, Amazon) was adhered to both sides of the VHB tape, and bubbles were removed using a flat edge of a piece of acrylic (Fig. 3C). Then, a CO<sub>2</sub> laser (ULS VLS2.30DT) was used to cut the board outline and the VIAs/header pin holes, using settings of 100% power and 20% speed, for two repetitions (Fig. 3D). Next, the top and bottom traces were cut into just the top and bottom pieces of circuit paper, respectively, with a UV laser (LPKF ProtoLaser U4, LPKF Inc.). The CO<sub>2</sub> laser, with a beam width of  $\sim 300 \mu\text{m}$ , efficiently cut through the substrate but had relatively low resolution. Conversely, the UV laser, with a beam width of  $15 \mu\text{m}$ , could cut precise, high-resolution mask traces but was unable to cut through the substrate. To ensure alignment, the board outline was cut into a piece of paper, and the circuit was then placed into the cutout in the paper top side up and taped in place. The top traces were then engraved into the mask (Fig. 3E). After flipping the circuit over its neutral axis and aligning in the paper cutout, the bottom traces were then engraved (Fig. 3F).

The pieces of sticker paper where the conductive material should go were removed with tweezers from the bottom side. The VIAs were filled with OGaIn using a sharp multimeter probe (FLUKE TP88). Then, OGaIn was painted into the mask using a paintbrush—brushing perpendicular to traces and in circles over them (Fig. 3G). Last, the edge of a piece of acrylic was used to scrape excess material off the top, and the mask was removed (Fig. 3H). Each trace was tested for conductivity using a two-point probe multimeter (FLUKE 83V) with the probes listed previously. For encapsulation, rubber cement was loaded into a syringe and extruded out of a 17-gauge needle over all exposed OGaIn (Fig. 3I).

Once the bottom side was cured, the same process was repeated until top mask removal (Fig. 3J), and components were placed exactly as they were on the rigid Pro Mini using tweezers. Wires were then placed with tweezers and adhered with Sil-Poxy (SmoothOn Inc.) (Fig. 3K). Next, a program was uploaded to the device to test for functionality. Last, the top was encapsulated, and the Sil-Poxy was added over the microprocessor and oscillator to create a strain gradient. Once cured, the circuit was tested again. Notes on improving and scaling this process can be found in Supplementary Methods.

The same process was used to make the other example circuits (SparkFun Sound Detector, Arduino Lilypad, and SparkFun RGB and Gesture Sensor), using their open-source designs. An extremely fine layer of Sil-Poxy was added to the bottom layer under the RGB sensor IC, and no encapsulant or Sil-Poxy was added directly over the lens.

## Circuit characterization

The five Arduino Pro Mini samples used for pull-to-failure tests were manufactured with a border on the edges such that fabric could be adhered, limiting the strain in those regions and ensuring that only the circuit board was straining. To set up, these fabric regions were gripped (Instron 2713-007) by the materials testing system (Instron 3345), and the wires for serial connection were plugged into an FTDI (Future Technology Devices International Limited) programming board (DEV-09716, SparkFun), which was connected to a laptop. A code that flashed four off-board LEDs and printed time stamps to the serial monitor was uploaded to the soft Pro Mini. The laptop and Arduino were recorded by an external camera setup. The Instron captured force and displacement data while it pulled upward at a rate of 15 mm/min until serial disconnect occurred. The initial length and length at failure of the circuit were calculated from the camera footage (with one initial frame and one frame just before serial disconnect), and from these, engineering strains were calculated. This same process was used to test the failure of the three additional example circuits, one sample each, although they were gripped with acrylic adhered to the circuit as the strain limiter. The Arduino Lilypad was strained until the LED stopped blinking at the rate specified in the script. The SparkFun Sound Detector was strained with loud ambient noise to detect the failure time. The SparkFun RGB and Gesture Sensor sent color output through serial until an error reading serial occurred. For all measurements in this paper, we chose to calculate the strain clamp to clamp (field standard) (17, 26–28, 36).

Cyclic testing of the soft Arduino Pro Minis used the same cyclic testing device as for the single-trace samples. The same additional grip areas were used, but instead of attaching fabric, laser-cut pieces of 3.18-mm acrylic were pressed onto either side of the excess VHB tape such that the four through holes fit onto the alignment pins of the cyclic tester (fig. S11). The cyclic tester strained to 100% strain for 1000 cycles, while a time-lapse camera monitored the laptop screen, which concurrently displayed the serial output from the soft circuit and the cycle number from the testing device. The number of cycles the circuit survived was recorded as the cycle before an error was seen in the serial output of the stretchable Arduino. After pull to failure and cyclic testing until serial disconnect, the samples were evaluated using the two-point probe FLUKE multimeter to determine where the failure occurred (fig. S7C).

To determine the effect the circuitry had on the circuit substrate's force-strain relationship, the same strain-limiting fabric pieces were attached to five stretchable Pro Mini circuits and five pieces of plain VHB tape. The materials testing system gripped these sections and strained each sample to 100% strain for 200 cycles at 15 mm/min. Data from cycles 1, 10 (after Mullin's effect) (57), and 200, straining and relaxing, were isolated for each sample. The means and SDs were then calculated for the five samples from cycles 1, 10, and 200, straining or relaxing.

## Fabrication and design of a quadruped

The soft quadruped robot was inspired by Shepherd *et al.* (8). The top portion of the robot was DS10 cast in a three-dimensional (3D) printed mold. Once cured, this top portion of the robot was placed onto fabric impregnated with uncured DS10, and the two parts cured together, with the bottom fabric acting as a strain-limiting layer. The bladders for the four legs and the body each had an exit to open air that, instead of being on the top, was out the sides. In these

exits, silicone tubes (5236 K203, McMaster-Carr) were inserted with tweezers and secured with Sil-Poxy.

To distribute the circuit design, the outline of the soft quadruped robot designed above was imported into AutoDesk Eagle as a board outline. The routing from the Arduino Pro Mini was then erased, the components manually moved to the desired locations on the board, and the autoroute feature in Eagle was used to create new routes, including GND lines.

The DS10 quadruped circuit was fabricated using the same manufacturing procedure, but Slacker 1.5 was used as the substrate and encapsulant (fig. S12A). For both the Slacker and VHB tape circuits, the I<sup>2</sup>C communication wires were added after the top was already encapsulated to ensure that no traces were bridged during wire placement. To do this, tweezers pinched the encapsulant above the header pin hole, and sewing scissors were used to snip a hole in the encapsulant. The wires were then attached the same way as described previously, and a dab of extra encapsulant was put over the wire lead.

The Slacker circuit was attached to the DS10 robot by coating a thin layer of DS10 over the top of the robot and placing the circuit on top to cure (fig. S12B). The VHB tape circuit adhered loosely to the robot, although the rubber cement did not adhere. At the tip of each leg, the circuit was mechanically bonded to the robot using DS10 (fig. S12, C and D).

The quadruped setup (movies S3 and S4) was as follows: The soft Arduino was connected to the laptop for the power supply and to the I<sup>2</sup>C breakout board. The breakout board was connected to the pressure regulators. Compressed air was fed into the pressure regulators, the outputs of which went to each leg and the body. The Arduino had a programmed gait that it ran by controlling the pressure regulators, using the I<sup>2</sup>C protocol.

### Fabrication and design of voxel robots

The voxel robots were composed of 16 voxels, each with dimensions of 15 mm by 15 mm by 60 mm, as fabricated and assembled in previous work (60, 61). Sil-Poxy was used to secure tubes in each bladder and apply friction-biased acrylic feet (fig. S13) to ensure 1D motion over the muslin fabric surface.

A stretchable LED array board was manufactured using the same method as the regular circuitry (fig. S8) and consisted of three LEDs (red, yellow, and green) and three 220-ohm resistors. The GNDs all connected to a point on the board that would be next to the GND pin on the Arduino when placed side by side. The three lines from the LEDs also came to their ends directly across from a set of digital pins on the Arduino. This board design was used for this demo and the wearable demo.

The stretchable Arduino and LED board were placed next to each other on top of each voxel robot, with an ~1-mm overlap between the sensing board and the Arduino so that the two boards would not separate when strained. Using tweezers to pull up the encapsulant and sewing scissors to cut it away, a digital pin, two GNDs, and pin A3 were exposed. Using a multimeter probe, OGAIn was painted from the digital pin on the Arduino to the LED trace on the breakout board and from GND to GND. These connections were then encapsulated. Next, the A3 pin was extended in the same manner, painting a path all the way to the top, front-facing voxel on the voxel bot, and covering that face (not encapsulating to maintain conductivity). The same was done to connect the other GND to the bottom voxel.

The soft Arduinos ran a code that spent half of the time listening for a 5-V signal and half of the time sending a 5-V signal. This way,

when the A3 and GND pins on each robot made contact with each other, they would light up the green LED. A valve connected to compressed air at 20 psi (138 kPa) was repeatedly opened and closed to get the two robots to inch toward each other.

### Fabrication and design of wearable system

A textile-based capacitive strain sensor, as developed in our previous work (65), was embedded into the elbow sleeve using the sleeve's fabric as a dielectric layer. The two leads from the sensor were soldered to a rigid capacitive sensor processing board (MPR121, Adafruit). From this board, 5-V, GND, and I<sup>2</sup>C lines were connected to the stretchable Arduino. Another LED breakout board was fabricated for this demonstration. The serial communication lines from the Pro Mini were connected to the FTDI programming board, which was connected through USB to a computer.

Laying the sleeve flat on a table, the Arduino was placed directly over the top of the sensor and pressed into place. The LED breakout board was placed next to it so that the GND and digital pins aligned and the substrate overlapped by 1 mm. The header pin holes for the three digital pins, LEDs, and GND were exposed on both the Arduino and the LED board, connected with more OGAIn, and then encapsulated with rubber cement.

### Statistical analysis

In each experiment, we have noted the number of times an experiment was independently performed ( $N$ ). Where  $N > 2$ , shaded regions or error bars indicate one SD. For fit lines,  $R^2$  values are reported. Units are listed for all measurements.

### Supplementary Materials

The PDF file includes:

Methods  
Figs. S1 to S13  
Table S1  
References (66, 67)

Other Supplementary Material for this manuscript includes the following:

Movies S1 to S7

### REFERENCES AND NOTES

1. Arduino Team, "The Arduino Forum is now completely renovated (and it's so nice)," 13 April 2021; <https://blog.arduino.cc/2021/04/13/the-arduino-forum-is-now-completely-renovated-and-its-so-nice/>.
2. Arduino, Uno R3; <https://docs.arduino.cc/hardware/uno-rev3/>.
3. M. T. Tolley, R. F. Shepherd, B. Mosadegh, K. C. Galloway, M. Wehner, M. Karpelson, R. J. Wood, G. M. Whitesides, A resilient, untethered soft robot. *Soft Robot.* **1**, 213–223 (2014).
4. M. P. Nemitz, P. Mihaylov, T. W. Barraclough, D. Ross, A. A. Stokes, Using voice coils to actuate modular soft robots: Wormbot, an example. *Soft Robot.* **3**, 198–204 (2016).
5. A. D. Marchese, C. D. Onal, D. Rus, Autonomous soft robotic fish capable of escape maneuvers using fluidic elastomer actuators. *Soft Robot.* **1**, 75–87 (2014).
6. A. A. Stokes, R. F. Shepherd, S. A. Morin, F. Ilievski, G. M. Whitesides, A hybrid combining hard and soft robots. *Soft Robot.* **1**, 70–74 (2014).
7. D. S. Shah, M. C. Yuen, L. G. Tilton, E. J. Yang, R. Kramer-Bottiglio, Morphing robots using robotic skins that sculpt clay. *IEEE Robot. Autom. Lett.* **4**, 2204–2211 (2019).
8. R. F. Shepherd, F. Ilievski, W. Choi, S. A. Morin, A. A. Stokes, A. D. Mazzeo, X. Chen, M. Wang, G. M. Whitesides, Multigait soft robot. *Proc. Natl. Acad. Sci. U.S.A.* **108**, 20400–20403 (2011).
9. S. Seok, C. D. Onal, K.-J. Cho, R. J. Wood, D. Rus, S. Kim, Meshworm: A peristaltic soft robot with antagonistic nickel titanium coil actuators. *IEEE/ASME Trans. Mechatron.* **18**, 1485–1497 (2013).
10. H. Yasuda, P. R. Buskohl, A. Gillman, T. D. Murphey, S. Stepney, R. A. Vaia, J. R. Raney, Mechanical computing. *Nature* **598**, 39–48 (2021).

11. D. Drotman, S. Jadhav, D. Sharp, C. Chan, M. T. Tolley, Electronics-free pneumatic circuits for controlling soft-legged robots. *Sci. Robot.* **6**, eaay2627 (2021).
12. D. J. Preston, P. Rothemund, H. J. Jiang, M. P. Nemitz, J. Rawson, Z. Suo, G. M. Whitesides, Digital logic for soft devices. *Proc. Natl. Acad. Sci. U.S.A.* **116**, 7750–7759 (2019).
13. M. Wehner, R. L. Truby, D. J. Fitzgerald, B. Mosadegh, G. M. Whitesides, J. A. Lewis, R. J. Wood, An integrated design and fabrication strategy for entirely soft, autonomous robots. *Nature* **536**, 451–455 (2016).
14. J. Wissman, M. D. Dickey, C. Majidi, Field-controlled electrical switch with liquid metal. *Adv. Sci.* **4**, 1700169 (2017).
15. W. Wu, Stretchable electronics: Functional materials, fabrication strategies and applications. *Sci. Technol. Adv. Mater.* **20**, 187–224 (2019).
16. D.-H. Kim, J. A. Rogers, Stretchable electronics: Materials strategies and devices. *Adv. Mater.* **20**, 4887–4892 (2008).
17. Z. Huang, Y. Hao, Y. Li, H. Hu, C. Wang, A. Nomoto, T. Pan, Y. Gu, Y. Chen, T. Zhang, W. Li, Y. Lei, N. Kim, C. Wang, L. Zhang, J. W. Ward, A. Maralani, X. Li, M. F. Durstock, A. Pisano, Y. Lin, S. Xu, Three-dimensional integrated stretchable electronics. *Nat. Electron.* **1**, 473–480 (2018).
18. S. Biswas, A. Schoeberl, Y. Hao, J. Reiprich, T. Stauden, J. Pezoldt, H. O. Jacobs, Integrated multilayer stretchable printed circuit boards paving the way for deformable active matrix. *Nat. Commun.* **10**, 4909 (2019).
19. S. I. Rich, R. J. Wood, C. Majidi, Untethered soft robotics. *Nat. Electron.* **1**, 102–112 (2018).
20. R. K. Kramer, C. Majidi, R. J. Wood, “Wearable tactile keypad with stretchable artificial skin” in *2011 IEEE International Conference on Robotics and Automation (IEEE)*, 2011, pp. 1103–1107.
21. M. D. Dickey, Stretchable and soft electronics using liquid metals. *Adv. Mater.* **29**, 1606425 (2017).
22. N. Kazem, T. Hellebrekers, C. Majidi, Soft multifunctional composites and emulsions with liquid metals. *Adv. Mater.* **29**, 1605985 (2017).
23. M. D. Bartlett, N. Kazem, M. J. Powell-Palm, X. Huang, W. Sun, J. A. Malen, C. Majidi, High thermal conductivity in soft elastomers with elongated liquid metal inclusions. *Proc. Natl. Acad. Sci. U.S.A.* **114**, 2143–2148 (2017).
24. N. Kazem, M. D. Bartlett, C. Majidi, Extreme toughening of soft materials with liquid metal. *Adv. Mater.* **30**, 1706594 (2018).
25. X. Yu, B. K. Mahajan, W. Shou, H. Pan, Materials, mechanics, and patterning techniques for elastomer-based stretchable conductors. *Micromachines* **8**, 7 (2017).
26. B. Lee, H. Cho, S. Moon, Y. Ko, Y.-S. Ryu, H. Kim, J. Jeong, S. Chung, Omnidirectional printing of elastic conductors for three-dimensional stretchable electronics. *Nat. Electron.* **6**, 307–318 (2023).
27. K. B. Ozutemiz, C. Majidi, O. B. Ozdoganlar, Scalable manufacturing of liquid metal circuits. *Adv. Mater. Technol.* **7**, 2200295 (2022).
28. K. B. Ozutemiz, J. Wissman, O. B. Ozdoganlar, C. Majidi, EGaN–metal interfacing for liquid metal circuitry and microelectronics integration. *Adv. Mater. Interfaces* **5**, 1701596 (2018).
29. L. Tang, S. Yang, K. Zhang, X. Jiang, Skin electronics from biocompatible in situ welding enabled by intrinsically sticky conductors. *Adv. Sci.* **9**, 2202043 (2022).
30. M. Tavakoli, P. A. Lopes, A. Hajjalou, A. F. Silva, M. R. Carneiro, J. Carvalho, J. M. Pereira, A. T. de Almeida, 3R electronics: Scalable fabrication of resilient, repairable, and recyclable soft-matter electronics. *Adv. Mater.* **34**, 2203266 (2022).
31. P. A. Lopes, D. F. Fernandes, A. F. Silva, D. G. Marques, A. T. de Almeida, C. Majidi, M. Tavakoli, Bi-phasic Ag-In-Ga-embedded elastomer inks for digitally printed, ultra-stretchable, multi-layer electronics. *ACS Appl. Mater. Interfaces* **13**, 14552 (2021).
32. P. A. Lopes, B. C. Santos, A. T. de Almeida, M. Tavakoli, Reversible polymer-gel transition for ultra-stretchable chip-integrated circuits through self-soldering and self-coating and self-healing. *Nat. Commun.* **12**, 4666 (2021).
33. W. Lee, H. Kim, I. Kang, H. Park, J. Jung, H. Lee, H. Park, J. S. Park, J. M. Yuk, S. Ryu, J.-W. Jeong, J. Kang, Universal assembly of liquid metal particles in polymers enables elastic printed circuit board. *Science* **378**, 637–641 (2022).
34. T. Hellebrekers, K. B. Ozutemiz, J. Yin, C. Majidi, “Liquid metal-microelectronics integration for a sensorized soft robot skin” in *IEEE International Conference on Intelligent Robots and Systems (IEEE)*, 2018, pp. 5924–5929.
35. J. Yin, T. Hellebrekers, C. Majidi, “Closing the loop with liquid-metal sensing skin for autonomous soft robot gripping” in *2020 3rd IEEE International Conference on Soft Robotics, RoboSoft (IEEE)*, 2020, pp. 661–667.
36. Z. Xie, F. Yuan, J. Liu, L. Tian, B. Chen, Z. Fu, S. Mao, T. Jin, Y. Wang, X. He, G. Wang, Y. Mo, X. Ding, Y. Zhang, C. Laschi, L. Wen, Octopus-inspired sensorized soft arm for environmental interaction. *Sci. Robot.* **8**, eadh7852 (2023).
37. S. Liu, D. S. Shah, R. Kramer-Bottiglio, Highly stretchable multilayer electronic circuits using biphasic gallium-indium. *Nat. Mater.* **20**, 851–858 (2021).
38. A. D. Valentine, T. A. Busbee, J. W. Boley, J. R. Raney, A. Chortos, A. Kotikian, J. D. Berrigan, M. F. Durstock, J. A. Lewi, Hybrid 3D printing of soft electronics. *Adv. Mater.* **29**, 1703817 (2017).
39. M. Tavakoli, M. H. Malakooti, H. Paisana, Y. Ohm, D. G. Marques, P. A. Lopes, A. P. Piedade, A. T. de Almeida, C. Majidi, EGaN-assisted room-temperature sintering of silver nanoparticles for stretchable, inkjet-printed, thin-film electronics. *Adv. Mater.* **30**, 1801852 (2018).
40. J. Wang, G. Cai, S. Li, D. Gao, J. Xiong, P. S. Lee, Printable superelastic conductors with extreme stretchability and robust cycling endurance enabled by liquid-metal particles. *Adv. Mater.* **30**, 1706157 (2018).
41. Y. Li, S. Feng, S. Cao, J. Zhang, D. Kong, Printable liquid metal microparticle ink for ultrastretchable electronics. *ACS Appl. Mater. Interfaces* **12**, 50852 (2020).
42. U. Daalkhajav, O. D. Yirmibesoglu, S. Walker, Y. Mengüç, Rheological modification of liquid metal for additive manufacturing of stretchable electronics. *Adv. Mater. Technol.* **3**, 1700351 (2018).
43. H. Chang, P. Zhang, R. Guo, Y. Cui, Y. Hou, Z. Sun, W. Rao, Recoverable liquid metal paste with reversible rheological characteristic for electronics printing. *ACS Appl. Mater. Interfaces* **12**, 14125 (2020).
44. D. H. Lee, T. Lim, J. Pyeon, H. Park, S.-W. Lee, S. Lee, W. Kim, M. Kim, J.-C. Lee, D.-W. Kim, S. Han, H. Kim, S. Park, Y.-K. Choi, Self-mixed biphasic liquid metal composite with ultra-high stretchability and strain-insensitivity for neuromorphic circuits. *Adv. Mater.* **36**, 2310956 (2024).
45. L. Sanchez-Botero, D. S. Shah, R. Kramer-Bottiglio, Are liquid metals bulk conductors? *Adv. Mater.* **34**, 2109427 (2022).
46. S. Zhu, J.-H. So, R. Mays, S. Desai, W. R. Barnes, B. Pourdeyhimi, M. D. Dickey, Ultrastretchable fibers with metallic conductivity using a liquid metal alloy core. *Adv. Funct. Mater.* **23**, 2308–2314 (2013).
47. W. Kong, N. U. H. Shah, T. V. Neumann, M. H. Vong, P. Kotagama, M. D. Dickey, R. Y. Wang, K. Rykaczewski, Oxide-mediated mechanisms of gallium foam generation and stabilization during shear mixing in air. *Soft Matter* **16**, 5801–5805 (2020).
48. X. Wang, L. Fan, J. Zhang, X. Sun, H. Chang, B. Yuan, R. Guo, M. Duan, J. Liu, Printed conformable liquid metal e-skin-enabled spatiotemporally controlled bioelectromagnetics for wireless multisite tumor therapy. *Adv. Funct. Mater.* **29**, 1907063 (2019).
49. T. Chen, J. Hu, K. Wang, K. Wang, W. Zhang, H. Xie, G. Gan, J. Shi, Oxygen vacancies in oxide-derived EGaN enhance CO<sub>2</sub> electrochemical reduction to CO in organic electrolyte. *Appl. Surf. Sci.* **612**, 155934 (2023).
50. ASTM International, “Standard test methods for vulcanized rubber and thermoplastic elastomers—Tension” (D412-16, ASTM, 2016); [www.astm.org/standards/d412](http://www.astm.org/standards/d412).
51. N. Zolfaghari, P. Khandagale, M. J. Ford, K. Dayal, C. Majidi, Network topologies dictate electromechanical coupling in liquid metal–elastomer composites. *Soft Matter* **16**, 8818–8825 (2020).
52. S. Lin, J. Xu, X. Zhi, D. Chen, J. Miao, P. B. Shull, D. Cui, Design and fabrication of a stretchable circuit board for wireless posture measurement. *IEEE Electron Device Lett.* **38**, 399–402 (2017).
53. D. G. Marques, P. A. Lopes, A. T. d. Almeida, C. Majidi, M. Tavakoli, Reliable interfaces for EGaN multi-layer stretchable circuits and microelectronics. *Lab Chip* **19**, 897–906 (2019).
54. F. Bueche, Molecular basis for the Mullins effect. *J. Appl. Polym. Sci.* **4**, 107–114 (1960).
55. I. D. Joshipura, K. A. Persson, V. K. Truong, J.-H. Oh, M. Kong, M. H. Vong, C. Ni, M. Alsafatwi, D. P. Parekh, H. Zhao, M. D. Dickey, Are contact angle measurements useful for oxide-coated liquid metals? *Langmuir* **37**, 10914–10923 (2021).
56. A. Cook, D. P. Parekh, C. Ladd, G. Kotwal, L. Panich, M. Durstock, M. D. Dickey, C. E. Tabor, Shear-driven direct-write printing of room-temperature gallium-based liquid metal alloys. *Adv. Eng. Mater.* **21**, 1900400 (2019).
57. L. Mullins, Softening of rubber by deformation. *Rubber Chem. Technol.* **42**, 339–362 (1969).
58. N. W. Bartlett, M. T. Tolley, J. T. B. Overvelde, J. C. Weaver, B. Mosadegh, K. Bertoldi, G. M. Whitesides, R. J. Wood, A 3D-printed, functionally graded soft robot powered by combustion. *Science* **349**, 161–165 (2015).
59. J. W. Booth, J. C. Case, E. L. White, D. S. Shah, R. Kramer-Bottiglio, “An addressable pneumatic regulator for distributed control of soft robots” in *2018 IEEE International Conference on Soft Robotics (RoboSoft)* (IEEE, 2018), pp. 25–30.
60. S. Kriegman, A. M. Nasab, D. Shah, H. Steele, G. Branin, M. Levin, J. Bongard, R. Kramer-Bottiglio, “Scalable sim-to-real transfer of soft robot designs” in *2020 3rd IEEE International Conference on Soft Robotics (RoboSoft)* (IEEE, 2020), pp. 359–366.
61. S. Kriegman, S. Walker, D. Shah, M. Levin, R. Kramer-Bottiglio, J. Bongard, “Automated shapeshifting for function recovery in damaged robots” in *Robotics: Science and Systems* (Robotics: Science and Systems Proceedings, 2019).
62. D. Shah, B. Yang, S. Kriegman, M. Levin, J. Bongard, R. Kramer-Bottiglio, Shape changing robots: Bioinspiration, simulation, and physical realization. *Adv. Mater.* **33**, 2002882 (2020).
63. A. Chortos, J. Liu, Z. Bao, Pursuing prosthetic electronic skin. *Nat. Mater.* **15**, 937–950 (2016).
64. M. D. Bartlett, E. J. Markvicka, C. Majidi, Rapid fabrication of soft, multilayered electronics for wearable biomonitoring. *Adv. Funct. Mater.* **26**, 8496–8504 (2016).
65. L. Sanchez-Botero, A. Agrawala, R. Kramer-Bottiglio, Stretchable, breathable, and washable fabric sensor for human motion monitoring. *Adv. Mater. Technol.* **8**, 2300378 (2023).

66. A. K. Battu, C. V. Ramana, Mechanical properties of nanocrystalline and amorphous gallium oxide thin films. *Adv. Eng. Mater.* **20**, 1701033 (2018).
67. G. Reeves, H. Harrison, Obtaining the specific contact resistance from transmission line model measurements. *IEEE Electron Device Lett.* **3**, 111–113 (1982).

**Acknowledgments:** We thank L. Sanchez-Botero for providing material for preliminary experiments and engaging in discussions. **Funding:** This material is based on work supported by the National Science Foundation under grant no. IIS-1954591. S.J.W. was supported by a NASA NSTGRO Fellowship (80NSSC22K1188). D.S.S. was supported by a NASA Space Technology Research Fellowship (80NSSC17K0164). A.A. was supported by an NSF Graduate Research Fellowship (DGE-2139841). **Author contributions:** R.K.-B. conceived the project. S.J.W. designed and executed all experiments and led the writing of the paper. D.S.S. developed the initial manufacturing procedure. D.S.S. and R.K.-B. contributed to the design of the experiments and data interpretation. M.L. contributed to fabricating and executing the quadruped and VoxelBot demonstrations. A.A. fabricated the sensor and helped execute the

wearable demonstration. All authors contributed to the preparation of the manuscript. **Competing interests:** S.J.W., D.S.S., and R.K.-B. are listed as inventors on US continuation-in-part application no. 18/148,500, which claims priority to US Patent application no. 17/357,060, on which D.S.S. and R.K.-B. are also inventors. All other authors declare that they have no competing interests. **Data and materials availability:** All data needed to evaluate the conclusions in this paper are present in the paper or the Supplementary Materials. The data and code for this study have been deposited in the Dryad database (<https://doi.org/10.5061/dryad.80gb5mkxf>), and additional resources, including design files, laser cutting files, a bill of materials, and step-by-step instructions for creating your own stretchable Arduino, are on GitHub at <https://github.com/swoodman11/SoftArduino>.

Submitted 21 December 2023

Accepted 12 August 2024

Published 11 September 2024

10.1126/scirobotics.adn6844